THE JOURNAL OF PHYSICAL CHEMISTRY C
A JOURNAL OF THE AMERICAN CHEMICAL SOCIETY

pubs.acs.org/JPCC
Article

Challenge of Small Energy Differences in Metal−Organic Framework Reactivity

Published as part of The Journal of Physical Chemistry C virtual special issue "Roland Lindh Festschrift".

Noah Dohrmann,[‖] Daniel S. King,[‖] Carlo A. Gaggioli, and Laura Gagliardi*

Cite This: *J. Phys. Chem. C* 2023, 127, 16891−16900

Read Online

ACCESS | Metrics & More | Article Recommendations | Supporting Information

ABSTRACT: Metal−organic frameworks (MOFs) offer a promising architecture for designing heterogeneous catalysts, in which catalytically active metal centers can be installed on a porous MOF structure and modified using nonstructural ligands. Recently, it was shown that the activity for ethylene hydrogenation of Ni deposited on the MOF NU-1000 can be amplified 26-fold via the use of substituted nonstructural benzoate ligands (Liu et al. *ACS Catal.* **2019**, *9*, 3198−3207). However, as profound as this result is experimentally, this change in activity corresponds to an activation energy difference of only about 2.4 kcal/mol, putting it at the edge of the accuracy of density functional theory. In this study, we evaluate various density functionals for their ability to provide a consistent description of the experimental trend using a single-metal approximation of the active site. Our findings demonstrate the difficulties faced when calculating trends in small energy differences in MOFs, such as variance between functionals and differences in predictions due to subtle geometrical or rovibrational effects. In summary, we find no agreement in even the sign of the trend between different functionals, and only a minority of functionals are able to reproduce the experimental trend. However, among the functionals we examined, a subset demonstrate robustness in their predictions (either in agreement with or against the experimental trend) and we recommend using them for the computation of these small energy differences in MOF catalysis.

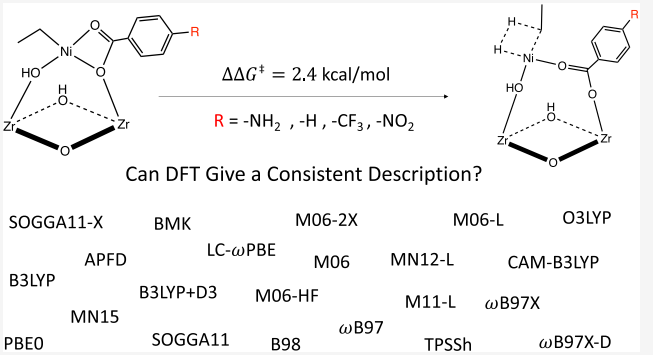

INTRODUCTION

Metal−organic frameworks (MOFs) are a broad class of porous materials consisting of inorganic nodes linked by organic linkers. By installing catalytically active metal centers on the nodes, MOFs have been shown to catalyze a variety of industrially relevant chemical reactions[1,2] such as ethylene hydrogenation,[3,4] propane oxidative hydrogenation,[5] alkene epoxidation,[6] and butene dimerization.[7,8] This activity can be enhanced further by tuning the metal centers via the use of nonstructural ligands.[2,3,9−13] In principle, this design allows for structurally controlled and modifiable metal centers to be integrated into a heterogeneous framework amenable to reuse. However, the central tasks of designing, synthesizing, and then functionalizing MOFs for catalysis are quite challenging,[14−16] and broad commercial-scale use is in many aspects still in the adoption phase. As such, computational modeling is critical to the development of this technology.[9,17] By far the most common approach to the modeling of catalytic MOF species is the use of density functional theory (DFT).[17,18] However, it is well known that descriptions of catalytic activity can vary depending on the choice of the density functional approximation.[17−19]

Despite this, it is generally hoped that although absolute differences in energies may vary between functional choices, trends in chemical activity are described consistently. However, this may not hold true when approaching the "chemical accuracy" limit (±1 kcal/mol) of DFT, as DFT tends to introduce errors of similar magnitude in benchmark data.[20] As trends in chemical activity approach this energy threshold, variations between functionals can become significant. Nevertheless, it is important to note that energy differences at this scale remain relevant, as a mere 2 kcal/mol energy difference corresponds to more than a tenfold change in catalytic activity at 100 °C. In the case of modeling small-molecular complexes, this sensitivity can often be mitigated by selecting a suitable functional based on comparison with benchmark wave

Received: June 8, 2023
Revised: July 31, 2023
Published: August 21, 2023

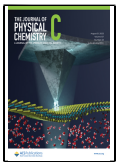

https://doi.org/10.1021/acs.jpcc.3c03888
J. Phys. Chem. C 2023, 127, 16891−16900

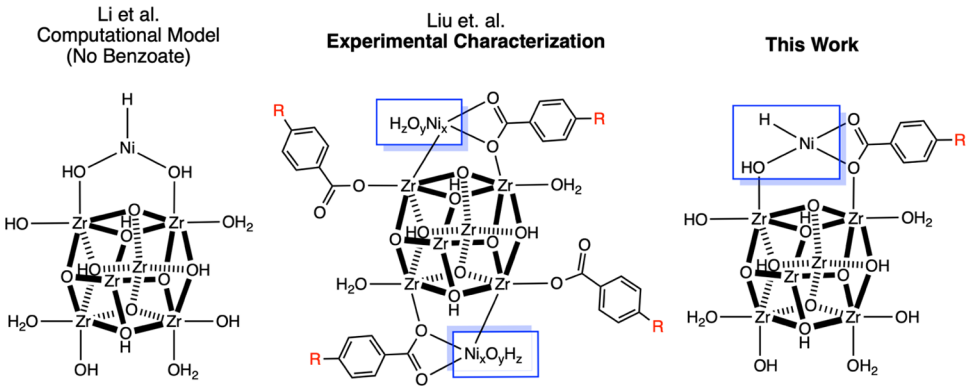

Figure 1. Left: Schematic of the cluster model used by Li et al.[3] to study the hydrogenation of ethylene by Ni deposited on NU-1000. Middle: Experimental characterization of a $Ni_xO_yH_z$ cluster by Liu and co-workers.[12] Right: Schematic of the modified cluster model used in this work to study the experimental trends. The bare node is composed of $Zr_6(\mu_3\text{-}O)_4(\mu_3\text{-}OH)_4(OH)_4(OH_2)_4$, which is linked to the other nodes in the MOF by eight 1,3,6,8-tetrakis(*p*-benzoate)pyrene linkers, which surround the node. In both models, these linkers are truncated to formate.[3]

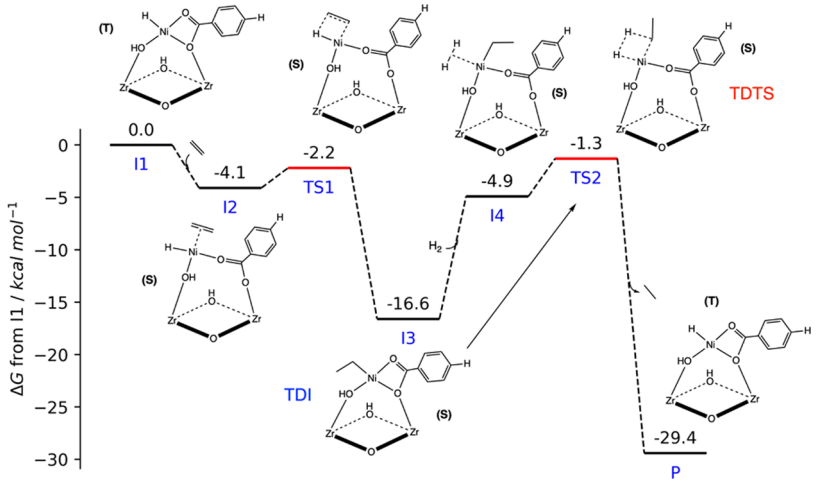

Figure 2. Calculated mechanism for ethylene hydrogenation on benzoate-modified Ni(II)-NU-1000, following the work of Li and co-workers.[3] Each structure is labeled as an intermediate (I) or transition state (TS, colored red) with numbers starting from 1 (**I1**, **I2**, **I3**) and (**TS1**, **TS2**) and further as a singlet (S) or triplet (T). The free energy of each structure relative to **I1** (calculated with M06-L) is shown above each label in kcal/mol. The product (**P**) represents the ΔG of ethane with respect to ethene and H_2. The TOF-determining intermediate (TDI) and TOF-determining transition state (TDTS) structures are identified as **I3** and **TS2**, respectively.

function theories.[21] However, in modeling extended inorganic complexes such as MOFs, this quickly becomes infeasible.

Recently, Liu and co-workers published a study in which a Hammett series of para-substituted benzoate nonstructural ligands (R = $-NH_2$, $-OCH_3$, $-CH_3$, $-H$, $-F$, $-NO_2$) were used to modify active Ni sites deposited on NU-1000[22,23] for ethylene hydrogenation, resulting in a 26-fold increase in activity from R = $-NO_2$ to R = $-OCH_3$.[12] While the effect of such substituted aryl species has been studied in MOF catalysis via replacement of the organic linkers,[24−29] studies on the direct modulation of the active site with such ligands remain to be done. Under the assumptions of transition state theory, the change in rate observed by Liu and co-workers corresponds to an activation energy difference of only 2.4 kcal/mol at the operating temperature of 100 °C, placing it at the edge of DFT chemical accuracy. Furthermore, the active site characterized by Liu and co-workers is ill-defined (a common trend in MOF catalysis), which makes it difficult to pin down an accurate computational model.

In this study, we employed 22 density functionals to investigate this experimental trend and assess the reliability of DFT in describing trends in MOFs at this energy scale using a single-metal approximation of the active site. Our results highlight the challenges encountered when computing trends in small energy differences in MOFs, such as variance between functionals and differences in predictions due to subtle geometrical or rovibrational effects. In summary, we find no agreement in even the sign of the trend between different functionals, and only a minority of functionals are able to reproduce the experimental trend. However, among the functionals we examined, a subset demonstrates robustness in their predictions (either in agreement with or against the experimental trend) and we recommend using them for the computation of these small energy differences in MOF catalysis.

METHODS

Our study begins from the work of Li et al.,[3] who computationally investigated ethylene hydrogenation by Ni deposited on bare NU-1000, without modification via nonstructural benzoate ligands. Figure 1 shows the active site model employed by Li et al.[3] (left), the experimental characterization of the active site by Liu and co-workers[12] (middle), and the model we have employed in this work

https://doi.org/10.1021/acs.jpcc.3c03888
J. Phys. Chem. C 2023, 127, 16891−16900

(right). To model the experimental trend, we have modified the Ni center of Li et al. by a single nonstructural para-substituted benzoate ligand.

However, we note that this use of a single Ni active site contradicts the experimental characterization of Liu and co-workers (Figure 1, middle), who experimentally characterized the active site as nondescript $Ni_xO_yH_z$ cluster with metal nuclearity close to 4 (and with an additional active site per node).[12] Although the use of such a cluster model would provide a more complete description, it has been shown in computational studies that Ni clusters have similar computed activity for ethylene oligomerization compared to single Ni centers on MOF nodes,[30] and thus we reasoned that a single Ni(II) active site was suitable for the purposes of this work.

Using this new catalytic model, the catalytic cycle of ethylene hydrogenation proposed by Li and co-workers was then reproduced in order to confirm the TOF-determining intermediate (TDI) and TOF-determining transition state (TDTS) (Figure 2). These computations were carried out with the M06-L functional[31] in Gaussian 16[32] using an ultrafine grid. The def2-SVP[33] basis set was used for nonmetals and def2-TZVPP[33,34] was used on Ni and Zr atoms. The SDD pseudopotential[34] was used for Zr to accelerate calculations, as used in previous studies of catalytic metals deposited on NU-1000.[35−37] Thermochemical effects were considered in the gas phase using standard rigid rotor harmonic oscillator (RRHO) approximations[38] at 100 °C, following the experimental report.[12] Low vibrational frequencies were treated with the quasi-harmonic treatment of Ribero et al.[39] with an applied scaling factor of 0.976 to the vibrational frequencies[40] as implemented in GoodVibes.[41] Linker carbon atoms were frozen in their initial positions during optimization.

Following these computations, the Hammett trend identified by Liu and co-workers was studied through computation of the TDI and TDTS energies for four para substituents: R = $-NH_2$, $-H$, $-CF_3$, and $-NO_2$. These energies were calculated by reoptimizing the geometries of the TDI and TDTS with 22 different density functionals (APFD,[42] B3LYP,[43] B3LYP+D3,[43,44] B98,[45,46] BMK,[47] CAM-B3LYP,[48] LC-ωPBE,[49] M06,[31] M06-2X,[50] M06-HF,[51,52] M06-L,[31] M11-L,[53] MN12-L,[54] MN15,[55] O3LYP,[56] PBE0,[57] SOGGA11,[58] SOGGA11-X,[59] TPSSh,[60,61] ωB97,[62] ωB97X,[62] and ωB97X-D[63]), which were chosen to present a good mix of hybrid functionals (e.g., B3LYP and M06), local functionals (e.g., M06-L, M11-L, and SOGGA11), functionals including dispersion (e.g., ωB97X-D and B3LYP+D3), and long-range corrected functionals (e.g., CAM-B3LYP and LC-ωPBE). We note that the substituents used to model the Hammett trend (R = $-NH_2$, $-H$, $-CF_3$, and $-NO_2$) differ slightly from those reported by Liu and co-workers (R = $-NH_2$, $-OCH_3$, $-CH_3$, $-H$, $-F$, and NO_2). We have chosen to replace R = $-OCH_3$, $-CH_3$, and $-F$ with R = $-CF_3$ in order to more efficiently screen the range of Hammett parameters and to avoid the conformational complications of R = $-OCH_3$.

To study the sensitivity of these trends with respect to thermochemical effects, enthalpies and entropies were calculated with different quasi-harmonic treatments of low vibrational modes. In the RRHO approximation, the entropy of a single vibrational mode is computed as

$$S_V = R\left[\frac{h\omega}{k(e^{h\omega/kT} - 1)} - \ln(1 - e^{-h\omega/kT})\right] \quad (1)$$

which is notoriously ill-behaved in the low-frequency limit of $\omega \to 0$. As such, several authors[39,64,65] have proposed quasi-harmonic treatments of low-frequency vibrations to avoid this behavior.

Table 1 shows the four treatments of low-frequency vibrations we investigate in this work, the first being the standard RRHO approach with the entropic contributions of all vibrational frequencies calculated via eq 1. The simple but effective approach proposed by Ribero et al.[39] is to replace all vibrational frequencies less than 100 with 100 cm^{-1}. Alternatively, Grimme[64] proposes an approach in which frequencies below 100 cm^{-1} are treated as rotations, and Li et al.[65] have proposed an additional quasi-harmonic treatment of these frequencies for enthalpic contributions. As will be shown, the use of these quasi-harmonic treatments can have significant effects on the predicted free-energy trends from DFT when small energy differences are under analysis. We note that an additional degree of freedom in computing thermochemical quantities from calculated vibrational frequencies is the use of empirical scaling factors.[40] However, due to the large amount of functionals used, no scaling factor was applied to the calculated frequencies in the larger investigation of the Hammett trends.

Table 1. Thermochemical Settings Used for the Calculation of Enthalpies and Free Energies[a]

scheme	name	description
1	RRHO	full harmonic treatment
2	Ribeiro	quasi-harmonic entropic correction of Ribero et al.[39]
3	Grimme	quasi-harmonic entropic correction of Grimme[64]
4	Li	both the quasi-harmonic entropic correction of Grimme and the quasi-harmonic enthalpic correction of Li et al.[65]

[a]All quasi-harmonic schemes use a cutoff frequency of 100 cm^{-1}.

RESULTS

Figure 2 shows the catalytic cycle computed for ethylene hydrogenation for benzoate-modified Ni deposited on NU-1000 computed with M06-L following the steps for the reaction on the bare node computed by Li and co-workers.[3] Starting from the Ni(II) hydride **I1**, an ethylene molecule binds to form **I2**, which then undergoes migratory insertion in **TS1** to form **I3**. Hydrogen then binds to form species **I4**, which undergoes another migratory insertion in **TS2** to form ethane (**P**). As Ni(II) has a formal d^8 electron configuration, it can occur both in the singlet ($M_s = 0$) and triplet ($M_s = 1$) spin states; besides the initial configuration **I1**, all structures were computed to be most stable as singlet states.

In contrast to the hydrogenation without benzoate computed by Li and co-workers,[3] our calculations suggest that the nonstructural benzoate stabilizes the Ni with respect to the bare node, alternating between chelating the bound Ni center with one or two oxygens. This reaction diagram clearly presents a single turnover frequency (TOF)-determining intermediate (TDI, **I3**) and TOF-determining transition state (TDTS, **TS2**) under the assumptions of the energetic span model,[66] which allows the proportionality of the TOF to be expressed as

$$\mathrm{TOF} \propto \exp\left[\frac{G_{TDI} - G_{TDTS}}{RT}\right] \quad (2)$$

https://doi.org/10.1021/acs.jpcc.3c03888
J. Phys. Chem. C 2023, 127, 16891−16900

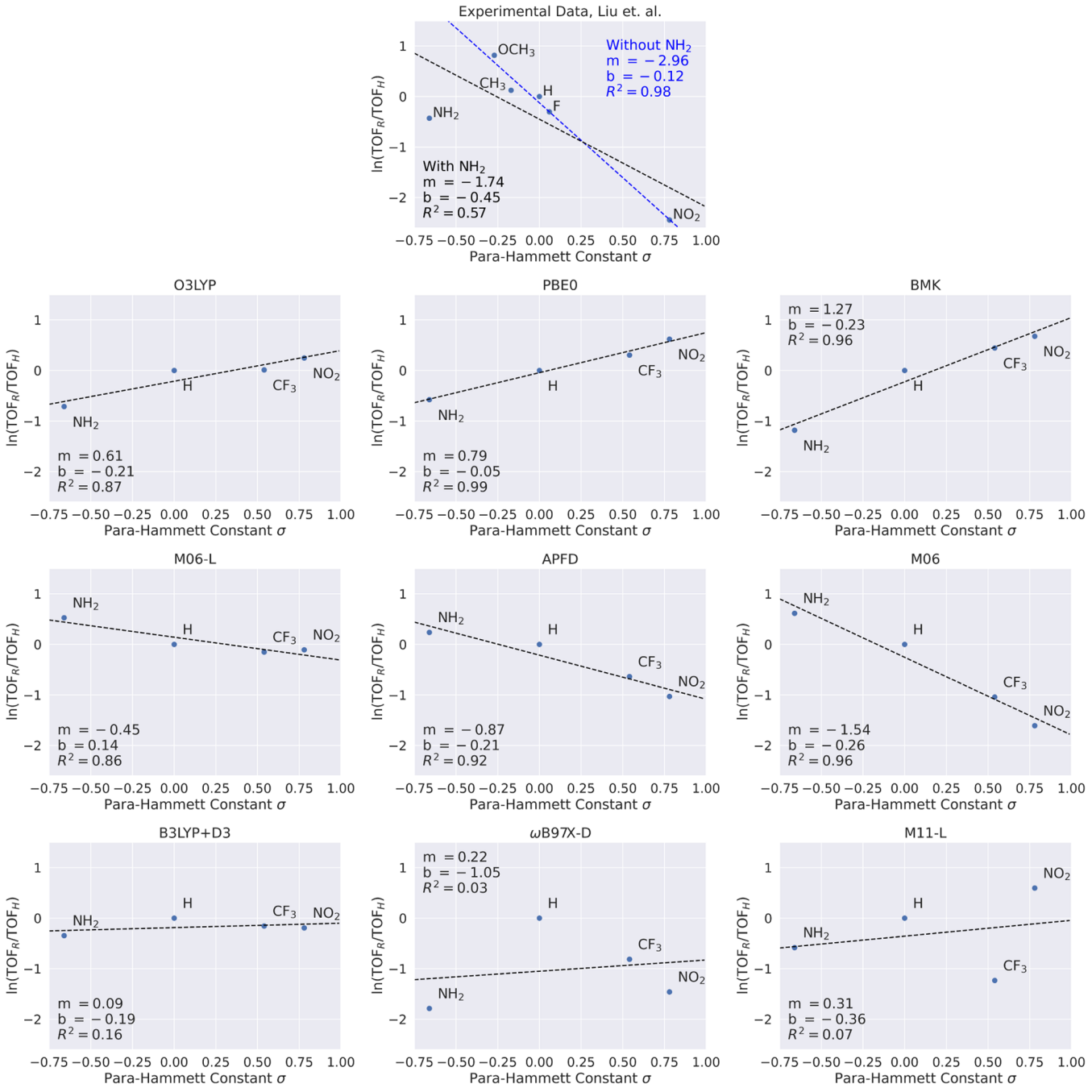

Figure 3. Top: Experimentally observed data by Liu and co-workers,[12] with lines of best fit both excluding R = $-NH_2$ (blue, as done in the original work) and including R = $-NH_2$ (black). Bottom: Trends in calculated catalytic activity calculated across the Hammett series of R = $-NH_2$, $-H$, $-CF_3$, and $-NO_2$ predicted by nine different density functionals (O3LYP, PBE0, BMK, M06-L, APFD, M06, B3LYP+D3, ωB97X-D, and M11-L) using eq 2 with the TDI and TDTS identified by M06-L (Figure 2) but reoptimized with each functional. Lines of best fit as a function of the Hammett constant σ ($m\sigma + b$) are shown in black for each functional, with slopes (m), intercepts (b), and R^2 values shown as text on each plot.

We use this relationship to compute trends in the relative TOF for different density functionals and quasi-harmonic treatments.

To give a sense of the variance we found in the computed trends among the different density functionals, Figure 3 shows the trends in catalytic activity predicted across the Hammett series of R = $-NH_2$, $-H$, $-CF_3$, and $-NO_2$ by nine of the 22 density functionals (O3LYP, PBE0, BMK, M06-L, APFD, M06, B3LYP+D3, ωB97X-D, and M11-L) using eq 2 with standard RRHO approximations. Lines of best fit as a function of the Hammett constant σ ($m\sigma + b$) are shown in black for each functional, with slopes (m), intercepts (b), and R^2 values shown as text on each plot. These trends are compared to the experimental data shown at the top of the figure. As can be seen, the predicted trends vary significantly between functionals, with three functionals giving positive slopes (O3LYP, PBE0, and BMK), three functionals giving negative slopes (M06-L, APFD, and M06), and three functionals giving a slope close to zero (B3LYP+D3, ωB97X-D, and M11-L).

Figure 4 shows the slopes (m) of lines of best fit and calculated R^2 values for the 22 density functionals studied in this work using the RRHO approximation to calculate free

https://doi.org/10.1021/acs.jpcc.3c03888
J. Phys. Chem. C 2023, 127, 16891−16900

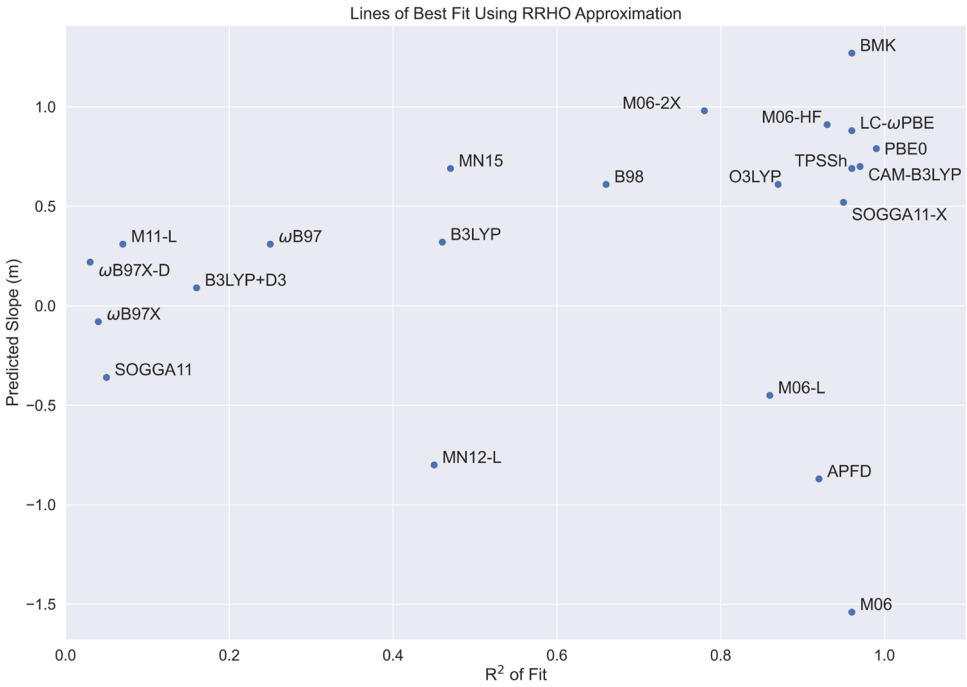

Figure 4. Slopes of lines of best fit and R^2 value for 22 functionals calculated across the Hammett series of R = $-NH_2$, $-H$, $-CF_3$, and $-NO_2$ using RRHO thermochemical approximations.

Figure 5. Slopes of lines of best fit and R^2 value across the Hammett series of R = $-NH_2$, $-H$, $-CF_3$, and $-NO_2$ that show variance in the strength and sign of predicted trends with different quasi-harmonic thermochemical approximations (Table 1).

energies. As can be seen, there is significant variance in the predicted trend between different functionals (m = −1.54 (M06) to m = +1.27 (BMK)). For the purposes of qualitatively analyzing the predictions of the different functionals, we separate those which predict a trend with $R^2 > 0.65$ (said to have a "significant" trend) from those which predict a trend with $R^2 < 0.65$ (said to have no significant trend). Of the 22 functionals investigated, 10 give significant positive slopes ($R^2 > 0.65$, $m > 0$), three give significant negative slopes ($R^2 > 0.65$, $m < 0$), and the remaining 9 functionals give no significant trend at all ($R^2 < 0.65$).

However, in some cases, this lack of significance is due to NH_2 being an outlier in the predicted trend (e.g., ωB97X-D in Figure 3), which is in qualitative agreement with the experimental results including NH2 (Figure 3, top). Unfortunately, due to variance between functionals, it is difficult to establish these predictions as more or less meaningful than functionals with different outlier groups (e.g., M11-L in Figure 3).

https://doi.org/10.1021/acs.jpcc.3c03888
J. Phys. Chem. C 2023, 127, 16891−16900

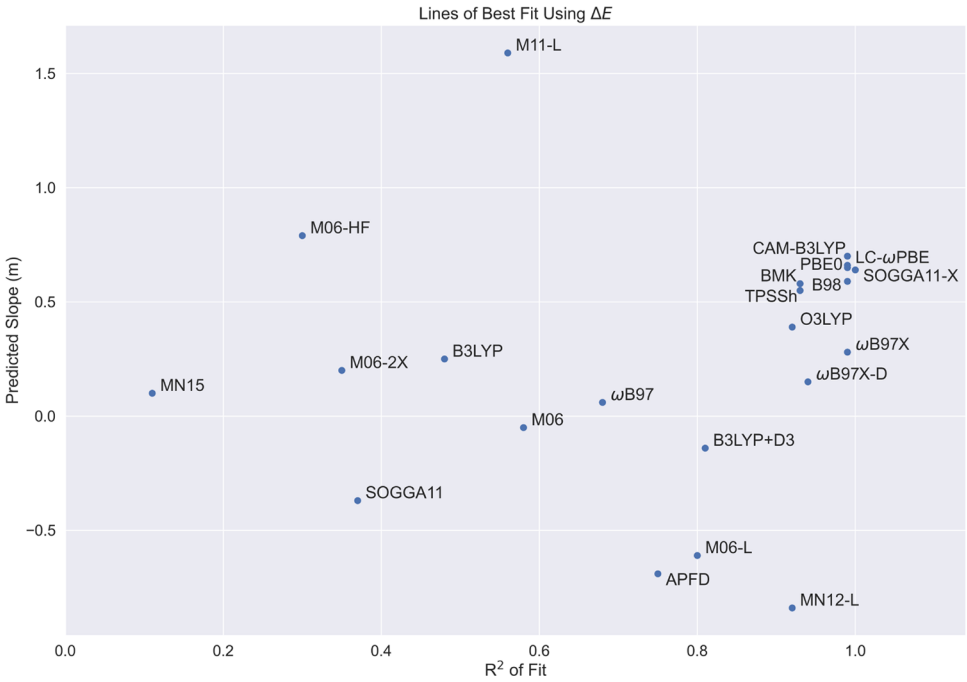

Figure 6. Slopes of lines of best fit and R^2 value across the Hammett series of R = $-NH_2$, $-H$, $-CF_3$, and $-NO_2$ using predictions from only differences in the electronic energy.

In analyzing trends between different functionals, there is little similarity to be found between the predictions of local (e.g., M11-L, M06-L), hybrid (e.g., ωB97X, M06-2X), high-parameter (e.g., M06, MN15), low-parameter (e.g., B3LYP, PBE0), dispersion-corrected (e.g., ωB97X-D, APFD), or long-range (e.g., ωB97, CAM-B3LYP) functionals—the sign and strength of the trend is distributed in all of these categories. For example, no trend can be found in the M06 series, in which the slope initially becomes more negative with increasing exact exchange (M06-L: $m = -0.45$ to M06: $m = -1.54$) but turns positive moving to M06-2X ($m = 0.98$) and M06-HF ($m = 0.93$).

Variance in DFT predictions is also found moving between different quasi-harmonic treatments (Figure 5). Moving from standard RRHO to the quasi-harmonic treatment of Ribero et. al., two functionals move from predicting significant positive trends with $R^2 > 0.65$ to predicting no significant trend at all: BMK ($R^2 = 0.96 \rightarrow R^2 = 0.09$) and M06-2X ($R^2 = 0.78 \rightarrow R^2 = 0.54$). Thus, in these functionals, the trend observed under the RRHO treatment of vibrational effects is primarily driven by the calculated entropies of vibrations less than 100 cm^{-1}. Expectantly, in both the case of BMK and M06-2X, the trend predicted under RRHO treatment returns gradually under the treatments of Grimme and Li and co-workers (BMK: $R^2 = 0.09 \rightarrow R^2 = 0.74$; M06-2X: $R^2 = 0.54 \rightarrow R^2 = 0.7$), which increasingly incorporate the thermochemical effects of vibrations under 100 cm^{-1} quasi-harmonically instead of eliminating them completely as is done under the approach of Ribero et al.

In other cases, functionals only predict significant trends ($R^2 > 0.65$) when quasi-harmonic treatment is added: B3LYP ($R^2 = 0.46 \rightarrow R^2 = 0.96$), MN12-L ($R^2 = 0.45 \rightarrow R^2 = 0.70$), and MN15 ($R^2 = 0.47 \rightarrow R^2 = 0.68$). Thus, in these functionals, the lack of a trend observed under the RRHO treatment of vibrational effects is primarily due to spurious thermochemical contributions to the calculated entropies of vibrations less than 100 cm^{-1}. Correspondingly, as the thermochemical effects of these frequencies are reincorporated quasi-harmonically, the strength of predicted trends is decreased: B3LYP ($R^2 = 0.96 \rightarrow R^2 = 0.71$), MN12-L ($R^2 = 0.7 \rightarrow R^2 = 0.54$), and to a lesser extent MN15 ($R^2 = 0.68 \rightarrow R^2 = 0.61$). The stark difference in this behavior between B3LYP and B3LYP+D3 is particularly noteworthy.

Given the variance in free-energy predictions, one might wish to examine trends in only the electronic portion of the energy directly predicted by DFT. Unfortunately, while this results in marked differences from the free-energy predictions, it does not appear to improve consistency between predictions. Figure 6 shows the computed trends with the approximation $\Delta\Delta G^{\ddagger} \approx \Delta\Delta E^{\ddagger}$.[67] Of the 22 functionals studied, 9 functionals give significant positive slopes ($R^2 > 0.65$, $m > 0$), four give significant negative slopes ($R^2 > 0.65$, $m < 0$), and the rest give no significant prediction ($R^2 < 0.65$). Overall, the size of predicted trends is decreased moving from the predictions using RRHO (Figure 4), with several functionals predicting slopes near $m = 0$.

Despite this, five functionals move to predicting significant trends when considering only changes in ΔE: B3LYP+D3 ($R^2 = 0.16 \rightarrow R^2 = 0.81$), MN12-L ($R^2 = 0.45 \rightarrow R^2 = 0.81$), ωB97 ($R^2 = 0.25 \rightarrow R^2 = 0.68$), ωB97X ($R^2 = 0.04 \rightarrow R^2 = 0.99$), and ωB97X-D ($R^2 = 0.03 \rightarrow R^2 = 0.94$), while three functionals move to predicting insignificant trends: M06 ($R^2 = 0.96 \rightarrow R^2 = 0.58$), M06-2X ($R^2 = 0.78 \rightarrow R^2 = 0.35$), and M06-HF ($R^2 = 0.93 \rightarrow R^2 = 0.3$). Thus, thermochemical corrections from the RRHO approximation are responsible for the predicted slope (or lack thereof) for many of the trends in free energy shown in Figure 4. The example of B3LYP+D3 is particularly surprising, as given the strong trends shown by B3LYP under quasi-harmonic treatment, this implicates the dispersive correction to the vibrational terms in accounting for the lack of trend in B3LYP+D3 (Figure 5).

https://doi.org/10.1021/acs.jpcc.3c03888
J. Phys. Chem. C 2023, 127, 16891−16900

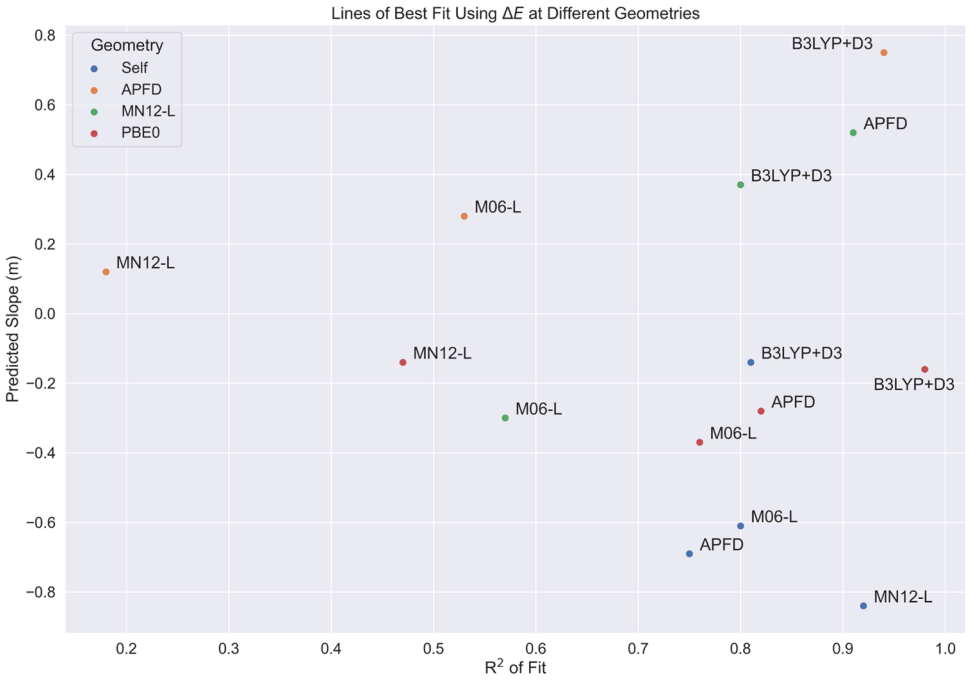

Figure 7. Slopes of lines of best fit and R^2 value across the Hammett series of R = $-NH_2$, $-H$, $-CF_3$, and $-NO_2$ using predictions from only differences in the electronic energy for M06-L, MN12-L, B3LYP+D3, and APFD, calculated using four different geometries: geometries optimized with the same functional used to calculate energy differences (M06-L, MN12-L, B3LYP+D3, and APFD, labeled as "Self"), geometries optimized with APFD, geometries optimized with MN12-L, and geometries optimized with PBE0. For APFD and MN12-L, only the "Self" point is shown instead of APFD and MN12-L, respectively.

To understand the sensitivity of these trends in the electronic energy to geometrical differences, we calculated single-point trends using geometries optimized with three different functionals: two functionals with $m < 0$ (APFD and MN12-L) and one functional with $m > 0$ (PBE0). These calculated trends are shown in Figure 7, for four functionals with particularly high variance in this regard: APFD, MN12-L, M06-L, and B3LYP+D3. As can be seen, the change in geometries between functionals can have dramatic effects on the predicted slope: APFD ($m = -0.69 \rightarrow m = 0.52$ at MN12-L geometries) and B3LYP+D3 ($m = -0.14 \rightarrow m = 0.75$ at APFD geometries) move from positive to negative slopes while maintaining significant R^2 values. Similarly, M06-L ($R^2 = 0.8 \rightarrow R^2 = 0.53$ at APFD geometries) and MN12-L ($R^2 = 0.92 \rightarrow R^2 = 0.18$ at APFD geometries) move from predicting significant trends to insignificant ones ($R^2 > 0.65 \rightarrow R^2 = 0.65$); the reverse is true of B3LYP ($R^2 = 0.48 \rightarrow R^2 = 0.99$ at PBE0 geometries), M06-2X ($R^2 = 0.35 \rightarrow R^2 = 0.99$ at PBE0 geometries), M06-HF ($R^2 = 0.30 \rightarrow R^2 = 1.00$ at PBE0 geometries), M11-L ($R^2 = 0.56 \rightarrow R^2 = 0.96$ at PBE0 geometries), and MN15 ($R^2 = 0.11 \rightarrow R^2 = 0.97$ at PBE0 geometries).

DISCUSSION AND CONCLUSIONS

In summary, we find the predictions of different DFT functionals to be scattered and inconsistent when utilizing a single-metal approximation of the active site studied by Liu et al.[12] About half of the functionals we tested predict a positive slope opposite to the experimental findings, while an equal amount predict a negative slope or no significant trend at all (Figure 4). Furthermore, the sign and strength of these trends are impacted significantly by the treatment of small thermochemical effects and geometrical contributions (Figures 5−7).

What can be taken away from these results? One possible conclusion is that our catalytic model (Figure 1) is incorrect. Although functionals vary in their predictions of the Hammett trend (with $m \in (-1.5, 1.5)$ kcal/σ), no functional predicts a slope similar in magnitude to the experimental value of $m = -2.96$ when treating NH_2 as an outlier (Figure 4). This might indicate a more active participation of the modified benzoate in the catalysis than is included in our catalytic model (Figure 1, right). A key approximation of our model is the treatment of the active site as a single-metal center, which contradicts the experimental characterization of the active site as a metal cluster.[12] It is possible that modeling the active site as a cluster allows for a more direct participation of the benzoate ligand in catalysis, perhaps in stabilizing a geometrical configuration of the nanocluster that carries out the catalysis. Alternatively, Ni clusters may enable a different catalytic pathway (e.g., hydrogen adsorption to the cluster) which allows for stronger electronic effects from the benzoate substituent. Additionally, unmodeled benzoate substituents bound to different sites (Figure 1, middle) or structural linkers (reduced to formate in our model) may have some effect. Evidently, to achieve reliable quantitative accuracy in the absolute barriers at this energy scale likely requires more careful experimental characterization of the active site and a correspondingly more detailed computational model.

On the other hand, a predicted slope of -1.5 kcal/σ is not far off from the experimental findings if one considers fitting to the outlier NH_2 data point excluded from the experimental fit ($m = -1.74$ kcal/σ and $R^2 = 0.57$). For example, M06 with standard RRHO thermochemistry predicts a nearly quantitatively identical slope ($m = -1.54$ kcal/σ) and ωB97X-D provides a trend in qualitative agreement with the experimental

https://doi.org/10.1021/acs.jpcc.3c03888
J. Phys. Chem. C 2023, 127, 16891−16900

findings where NH_2 is predicted to be an outlier point (Figure 3). Furthermore, the single-metal model would seem to provide a good model for directly examining the electronic effects of the benzoate substituent, as the substituted benzoate ligand is directly connected to the active metal site. While it is impossible to say whether or not another catalytic model is capable of convincingly reproducing the experimental trends using DFT, we view the takeaway of our work to be that given a reasonable (albeit limited) single-metal approximation for interrogating the trends observed in the Hammett series, DFT fails to give a consistent description of even the sign of the trend. One must be wary when evaluating trends on extended systems in magnitude close to the accuracy limit of DFT (±1 kcal/mol).

However, our calculations provide a few key takeaways of practical value. First, we find that at this energy scale, thermochemical contributions play a key role—the magnitude of trends is significantly reduced when neglecting rovibrational effects and evaluating only changes in the electronic energy (Figure 4 vs Figure 6). Despite this, noise from rovibrational effects may result in a lack of any trend at this energy scale, as found for the ωB97 family of functionals. Thus, for investigating trends at this energy scale, we suggest functionals that from our screening produce significant R^2 values (>0.65) in both $\Delta G^{\ddagger}$ and $\Delta E^{\ddagger}$, without varying significantly depending on thermochemical settings: APFD, B98, CAM-B3LYP, LC-ωPBE, M06-L, O3LYP, PBE0, SOGGA11-X, and TPSSh. Among these, APFD and M06-L show particular sensitivity to the use of geometries optimized with different functionals, and one may wish to exclude these on that account. Alternatively, if one is convinced by the validity of our catalytic model, then it is worth mentioning the functionals that reproduce the sign of the experimental trend in all (quasi)harmonic treatments: APFD, M06, and M06-L. Regardless, we hope this work serves as a useful example to practitioners of DFT of the challenges that occur in the computational study of extended inorganic systems such as MOFs at small energy scales.

■ ASSOCIATED CONTENT

Supporting Information

The Supporting Information is available free of charge at https://pubs.acs.org/doi/10.1021/acs.jpcc.3c03888.

Analysis of trends in charge densities. Full XYZ coordinates of all cluster models (ZIP)

Tables of the data presented in Figures 4−7 (PDF)

■ AUTHOR INFORMATION

Corresponding Author

Laura Gagliardi − *Department of Chemistry, Pritzker School of Molecular Engineering, The James Franck Institute, and Chicago Center for Theoretical Chemistry, University of Chicago, Chicago, Illinois 60637, United States;* orcid.org/0000-0001-5227-1396; Email: lgagliardi@uchicago.edu

Authors

Noah Dohrmann − *The College, University of Chicago, Chicago, Illinois 60637, United States*

Daniel S. King − *Department of Chemistry, University of Chicago, Chicago, Illinois 60637, United States;* orcid.org/0000-0003-0208-5274

Carlo A. Gaggioli − *Department of Chemistry, University of Chicago, Chicago, Illinois 60637, United States;* orcid.org/0000-0001-9105-8731

Complete contact information is available at: https://pubs.acs.org/10.1021/acs.jpcc.3c03888

Author Contributions

‖N.D. and D.K. contributed equally to this work.

Notes

The authors declare no competing financial interest.

■ ACKNOWLEDGMENTS

This work was supported as part of the Catalyst Design for Decarbonization Center, an Energy Frontier Research Center funded by the U.S. Department of Energy, Office of Science, Basic Energy Sciences under Award No. DE-SC0023383. The authors thank the James Franck Institute for funding via the Summer Undergraduate Research Award and the Resource Computing Center of the University of Chicago for computational resources. Additionally, they thank the Minnesota supercomputing institute (MSI) for access to computational resources.

■ REFERENCES

(1) Rogge, S. M.; Bavykina, A.; Hajek, J.; Garcia, H.; Olivos-Suarez, A. I.; Sepúlveda-Escribano, A.; Vimont, A.; Clet, G.; Bazin, P.; Kapteijn, F.; et al. Metal−Organic and Covalent Organic Frameworks as Single-Site Catalysts. *Chem. Soc. Rev.* **2017**, *46*, 3134−3184.

(2) Wei, Y.-S.; Zhang, M.; Zou, R.; Xu, Q. Metal−Organic Framework-Based Catalysts With Single Metal Sites. *Chem. Rev.* **2020**, *120*, 12089−12174.

(3) Li, Z.; Schweitzer, N. M.; League, A. B.; Bernales, V.; Peters, A. W.; Getsoian, A.; Wang, T. C.; Miller, J. T.; Vjunov, A.; Fulton, J. L.; Lercher, J. A.; Cramer, C. J.; Gagliardi, L.; Hupp, J. T.; Farha, O. K. Sintering-Resistant Single-Site Nickel Catalyst Supported by Metal−Organic Framework. *J. Am. Chem. Soc.* **2016**, *138*, 1977−1982. PMID: 26836273

(4) Wang, X.; Zhang, X.; Pandharkar, R.; Lyu, J.; Ray, D.; Yang, Y.; Kato, S.; Liu, J.; Wasson, M. C.; Islamoglu, T.; et al. Insights Into the Structure−Activity Relationships in Metal−Organic Framework-Supported Nickel Catalysts for Ethylene Hydrogenation. *ACS Catal.* **2020**, *10*, 8995−9005.

(5) Li, Z.; Peters, A. W.; Bernales, V.; Ortuño, M. A.; Schweitzer, N. M.; DeStefano, M. R.; Gallington, L. C.; Platero-Prats, A. E.; Chapman, K. W.; Cramer, C. J.; et al. Metal−Organic Framework Supported Cobalt Catalysts for the Oxidative Dehydrogenation of Propane at Low Temperature. *ACS Cent. Sci.* **2017**, *3*, 31−38.

(6) Ahn, S.; Nauert, S. L.; Hicks, K. E.; Ardagh, M. A.; Schweitzer, N. M.; Farha, O. K.; Notestein, J. M. Demonstrating the Critical Role of Solvation in Supported Ti and Nb Epoxidation Catalysts via Vapor-Phase Kinetics. *ACS Catal.* **2020**, *10*, 2817−2825.

(7) Zheng, J.; Löbbert, L.; Chheda, S.; Khetrapal, N.; Schmid, J.; Gaggioli, C. A.; Yeh, B.; Bermejo-Deval, R.; Motkuri, R. K.; Balasubramanian, M.; et al. Metal-Organic Framework Supported Single-Site Nickel Catalysts for Butene Dimerization. *J. Catal.* **2022**, *413*, 176−183.

(8) Löbbert, L.; Chheda, S.; Zheng, J.; Khetrapal, N.; Schmid, J.; Zhao, R.; Gaggioli, C. A.; Camaioni, D. M.; Bermejo-Deval, R.; Gutiérrez, O. Y.; et al. Influence of 1-Butene Adsorption on the Dimerization Activity of Single Metal Cations on UiO-66 Nodes. *J. Am. Chem. Soc.* **2023**, *145*, 1407−1422.

(9) Bernales, V.; League, A. B.; Li, Z.; Schweitzer, N. M.; Peters, A. W.; Carlson, R. K.; Hupp, J. T.; Cramer, C. J.; Farha, O. K.; Gagliardi, L. Computationally Guided Discovery of a Catalytic Cobalt-Decorated Metal−Organic Framework for Ethylene Dimerization. *J. Phys. Chem. C* **2016**, *120*, 23576−23583.

(10) Yang, D.; Momeni, M. R.; Demir, H.; Pahls, D. R.; Rimoldi, M.; Wang, T. C.; Farha, O. K.; Hupp, J. T.; Cramer, C. J.; Gates, B. C.; et al. Tuning the Properties of Metal−Organic Framework Nodes as Supports of Single-Site Iridium Catalysts: Node Modification by Atomic Layer Deposition of Aluminium. *Faraday Discuss.* **2017**, *201*, 195−206.
(11) Goetjen, T. A.; Zhang, X.; Liu, J.; Hupp, J. T.; Farha, O. K. Metal−Organic Framework Supported Single Site Chromium (III) Catalyst for Ethylene Oligomerization at Low Pressure and Temperature. *ACS Sustainable Chem. Eng.* **2019**, *7*, 2553−2557.
(12) Liu, J.; Li, Z.; Zhang, X.; Otake, K. I.; Zhang, L.; Peters, A. W.; Young, M. J.; Bedford, N. M.; Letourneau, S. P.; Mandia, D. J.; Elam, J. W.; Farha, O. K.; Hupp, J. T. Introducing Nonstructural Ligands to Zirconia-Like Metal-Organic Framework Nodes to Tune the Activity of Node-Supported Nickel Catalysts for Ethylene Hydrogenation. *ACS Catal.* **2019**, *9*, 3198−3207.
(13) Chen, Y.; Ahn, S.; Mian, M. R.; Wang, X.; Ma, Q.; Son, F. A.; Yang, L.; Ma, K.; Zhang, X.; Notestein, J. M.; et al. Modulating Chemical Environments of Metal−Organic Framework-Supported Molybdenum (VI) Catalysts for Insights Into the Structure−Activity Relationship in Cyclohexene Epoxidation. *J. Am. Chem. Soc.* **2022**, *144*, 3554−3563.
(14) Meilikhov, M.; Yusenko, K.; Esken, D.; Turner, S.; Van Tendeloo, G.; Fischer, R. A. Metals@ MOFs−loading MOFs with metal nanoparticles for hybrid functions. *Eur. J. Inorg. Chem.* **2010**, *2010*, 3701−3714.
(15) Hendon, C. H.; Rieth, A. J.; Korzynski, M. D.; Dinca, M. Grand Challenges and Future Opportunities for Metal−Organic Frameworks. *ACS Cent. Sci.* **2017**, *3*, 554−563.
(16) Lorignon, F.; Gossard, A.; Carboni, M. Hierarchically Porous Monolithic MOFs: An Ongoing Challenge for Industrial-Scale Effluent Treatment. *Chem. Eng. J.* **2020**, *393*, No. 124765.
(17) Bernales, V.; Ortuño, M. A.; Truhlar, D. G.; Cramer, C. J.; Gagliardi, L. Computational Design of Functionalized Metal−Organic Framework Nodes for Catalysis. *ACS Cent. Sci.* **2018**, *4*, 5−19.
(18) Mancuso, J. L.; Mroz, A. M.; Le, K. N.; Hendon, C. H. Electronic Structure Modeling of Metal−Organic Frameworks. *Chem. Rev.* **2020**, *120*, 8641−8715.
(19) Gaggioli, C. A.; Stoneburner, S. J.; Cramer, C. J.; Gagliardi, L. Beyond Density Functional Theory: The Multiconfigurational Approach to Model Heterogeneous Catalysis. *ACS Catal.* **2019**, *9*, 8481−8502.
(20) Mardirossian, N.; Head-Gordon, M. Thirty Years of Density Functional Theory in Computational Chemistry: An Overview and Extensive Assessment of 200 Density Functionals. *Mol. Phys.* **2017**, *115*, 2315−2372.
(21) Wheeler, S. E.; McNeil, A. J.; Müller, P.; Swager, T. M.; Houk, K. Probing Substituent Effects in Aryl- Aryl Interactions Using Stereoselective Diels- Alder Cycloadditions. *J. Ame. Chem. Soc.* **2010**, *132*, 3304−3311.
(22) Mondloch, J. E.; Bury, W.; Fairen-Jimenez, D.; Kwon, S.; DeMarco, E. J.; Weston, M. H.; Sarjeant, A. A.; Nguyen, S. T.; Stair, P. C.; Snurr, R. Q.; et al. Vapor-Phase Metalation by Atomic Layer Deposition in a Metal−Organic Framework. *J. Am. Chem. Soc.* **2013**, *135*, 10294−10297.
(23) Planas, N.; Mondloch, J. E.; Tussupbayev, S.; Borycz, J.; Gagliardi, L.; Hupp, J. T.; Farha, O. K.; Cramer, C. J. Defining the Proton Topology of the Zr6-Based Metal−Organic Framework NU-1000. *J. Phys. Chem. Lett.* **2014**, *5*, 3716−3723.
(24) Vermoortele, F.; Vandichel, M.; Van de Voorde, B.; Ameloot, R.; Waroquier, M.; Van Speybroeck, V.; De Vos, D. E. Electronic Effects of Linker Substitution on Lewis Acid Catalysis with Metal−Organic Frameworks. *Angew. Chem., Int. Ed.* **2012**, *51*, 4887−4890.
(25) Katz, M. J.; Moon, S.-Y.; Mondloch, J. E.; Beyzavi, M. H.; Stephenson, C. J.; Hupp, J. T.; Farha, O. K. Exploiting parameter space in MOFs: a 20-fold enhancement of phosphate-ester hydrolysis with UiO-66-NH 2. *Chem. Sci.* **2015**, *6*, 2286−2291.
(26) Katz, M. J.; Klet, R. C.; Moon, S.-Y.; Mondloch, J. E.; Hupp, J. T.; Farha, O. K. One Step Backward is Two Steps Forward: Enhancing the Hydrolysis Rate of UiO-66 by Decreasing [OH−]. *ACS Catal.* **2015**, *5*, 4637−4642.
(27) Islamoglu, T.; Ortuño, M. A.; Proussaloglou, E.; Howarth, A. J.; Vermeulen, N. A.; Atilgan, A.; Asiri, A. M.; Cramer, C. J.; Farha, O. K. Presence Versus Proximity: the Role of Pendant Amines in the Catalytic Hydrolysis of a Nerve Agent Simulant. *Angew. Chem., Int. Ed.* **2018**, *57*, 1949−1953.
(28) Wu, J.; Wang, Z.; Jin, X.; Zhang, S.; Li, T.; Zhang, Y.; Xing, H.; Yu, Y.; Zhang, H.; Gao, X.; et al. Hammett Relationship in Oxidase-Mimicking Metal−Organic Frameworks Revealed Through a Protein-Engineering-Inspired Strategy. *Adv. Mater.* **2021**, *33*, No. 2005024.
(29) Wang, Z.; Meng, H.; Gao, X. J.; Zheng, J.-J.; Gao, X. Remote Substituent Effects on Catalytic Activity of Metal-Organic Frameworks: a Linker Orbital Energy Model. *Npj Comput. Mater.* **2023**, *9*, 59.
(30) Ye, J.; Gagliardi, L.; Cramer, C. J.; Truhlar, D. G. Single Ni Atoms and Ni4 Clusters Have Similar Catalytic Activity for Ethylene Dimerization. *J. Catal.* **2017**, *354*, 278−286.
(31) Zhao, Y.; Truhlar, D. G. A New Local Density Functional for Main-Group Thermochemistry, Transition Metal Bonding, Thermochemical Kinetics, and Noncovalent Interactions. *J. Chem. Phys.* **2006**, *125*, No. 194101.
(32) Frisch, M. J.; Trucks, G. W.; Schlegel, H. B.; Scuseria, G. E.; Robb, M. A.; Cheeseman, J. R.; Scalmani, G.; Barone, V.; Petersson, G. A.; Nakatsuji, H.; Li, X.; Caricato, M.; Marenich, A. V.; Bloino, J.; Janesko, B. G.; Gomperts, R.; Mennucci, B.; Hratchian, H. P.; Ortiz, J. V.; Izmaylov, A. F.; Sonnenberg, J. L.; Williams-Young, D.; Ding, F.; Lipparini, F.; Egidi, F.; Goings, J.; Peng, B.; Petrone, A.; Henderson, T.; Ranasinghe, D.; Zakrzewski, V. G.; Gao, J.; Rega, N.; Zheng, G.; Liang, W.; Hada, M.; Ehara, M.; Toyota, K.; Fukuda, R.; Hasegawa, J.; Ishida, M.; Nakajima, T.; Honda, Y.; Kitao, O.; Nakai, H.; Vreven, T.; Throssell, K.; Montgomery, J. A.; Peralta, J. E.; Ogliaro, F.; Bearpark, M. J.; Heyd, J. J.; Brothers, E. N.; Kudin, K. N.; Staroverov, V. N.; Keith, T. A.; Kobayashi, R.; Normand, J.; Raghavachari, K.; Rendell, A. P.; Burant, J. C.; Iyengar, S. S.; Tomasi, J.; Cossi, M.; Millam, J. M.; Klene, M.; Adamo, C.; Cammi, R.; Ochterski, J. W.; Martin, R. L.; Morokuma, K.; Farkas, O.; Foresman, J. B.; Fox, D. J. *Gaussian 16*, Revision C.01, 2016.
(33) Weigend, F.; Ahlrichs, R. Balanced Basis Sets of Split Valence, Triple Zeta Valence and Quadruple Zeta Valence Quality for H to Rn: Design and Assessment of Accuracy. *Phys. Chem. Chem. Phys.* **2005**, *7*, 3297−3305.
(34) Andrae, D.; Haeussermann, U.; Dolg, M.; Stoll, H.; Preuss, H. Energy-Adjustedab Initio Pseudopotentials for the Second and Third Row Transition Elements. *Theor. Chim. Acta* **1990**, *77*, 123−141.
(35) Gaggioli, C. A.; Sauer, J.; Gagliardi, L. Hydrogen Atom or Proton Coupled Electron Transfer? C−H Bond Activation by Transition-Metal Oxides. *J. Am. Chem. Soc.* **2019**, *141*, 14603−14611.
(36) Simons, M. C.; Ortuño, M. A.; Bernales, V.; Gaggioli, C. A.; Cramer, C. J.; Bhan, A.; Gagliardi, L. C−H Bond Activation on Bimetallic Two-Atom Co-M Oxide Clusters Deposited on Zr-Based MOF Nodes: Effects of Doping at the Molecular Level. *ACS Catal.* **2018**, *8*, 2864−2869.
(37) Yang, D.; Gaggioli, C. A.; Ray, D.; Babucci, M.; Gagliardi, L.; Gates, B. C. Tuning Catalytic Sites on Zr6O8 Metal−Organic Framework Nodes via Ligand and Defect Chemistry Probed With Tert-Butyl Alcohol Dehydration to Isobutylene. *J. Am. Chem. Soc.* **2020**, *142*, 8044−8056.
(38) Cramer, C. J. *Essentials of Computational Chemistry: Theories and Models*; John Wiley & Sons, 2013.
(39) Ribeiro, R. F.; Marenich, A. V.; Cramer, C. J.; Truhlar, D. G. Use of Solution-Phase Vibrational Frequencies in Continuum Models for the Free Energy of Solvation. *J. Phys. Chem. B* **2011**, *115*, 14556−14562.
(40) Alecu, I. M.; Zheng, J.; Zhao, Y.; Truhlar, D. G. Computational Thermochemistry: Scale Factor Databases and Scale Factors for Vibrational Frequencies Obtained From Electronic Model Chemistries. *J. Chem. Theory Comput.* **2010**, *6*, 2872−2887.

https://doi.org/10.1021/acs.jpcc.3c03888
J. Phys. Chem. C 2023, 127, 16891−16900

(41) Luchini, G.; Alegre-Requena, J.; Funes-Ardoiz, I.; Paton, R. S. GoodVibes: Automated Thermochemistry for Heterogeneous Computational Chemistry Data. *F1000Research* **2020**, *9*, No. 291.
(42) Austin, A.; Petersson, G. A.; Frisch, M. J.; Dobek, F. J.; Scalmani, G.; Throssell, K. A Density Functional With Spherical Atom Dispersion Terms. *J. Chem. Theory Comput.* **2012**, *8*, 4989−5007.
(43) Stephens, P. J.; Devlin, F. J.; Chabalowski, C. F.; Frisch, M. J. Ab Initio Calculation of Vibrational Absorption and Circular Dichroism Spectra Using Density Functional Force Fields. *J. Phys. Chem. A* **1994**, *98*, 11623−11627.
(44) Grimme, S.; Antony, J.; Ehrlich, S.; Krieg, H. A Consistent and Accurate Ab Initio Parametrization of Density Functional Dispersion Correction (DFT-D) for the 94 Elements H-Pu. *J. Chem. Phys.* **2010**, *132*, No. 154104.
(45) Becke, A. D. Density-Functional Thermochemistry. V. Systematic Optimization of Exchange-Correlation Functionals. *J. Chem. Phys.* **1997**, *107*, 8554−8560.
(46) Schmider, H. L.; Becke, A. D. Optimized Density Functionals From the Extended G2 Test Set. *J. Chem. Phys.* **1998**, *108*, 9624−9631.
(47) Boese, A. D.; Martin, J. M. Development of Density Functionals for Thermochemical Kinetics. *J. Chem. Phys.* **2004**, *121*, 3405−3416.
(48) Yanai, T.; Tew, D. P.; Handy, N. C. A New Hybrid Exchange−Correlation Functional Using the Coulomb-Attenuating Method (CAM-B3LYP). *Chem. Phys. Lett.* **2004**, *393*, 51−57.
(49) Henderson, T. M.; Izmaylov, A. F.; Scalmani, G.; Scuseria, G. E. Can Short-Range Hybrids Describe Long-Range-Dependent Properties? *J. Chem. Phys.* **2009**, *131*, No. 044108.
(50) Zhao, Y.; Truhlar, D. G. The M06 Suite of Density Functionals for Main Group Thermochemistry, Thermochemical Kinetics, Noncovalent Interactions, Excited States, and Transition Elements: Two New Functionals and Systematic Testing of Four M06-Class Functionals and 12 Other Functionals. *Theor. Chem. Acc.* **2008**, *120*, 215−241.
(51) Zhao, Y.; Truhlar, D. G. Comparative DFT Study of Van Der Waals Complexes: Rare-Gas Dimers, Alkaline-Earth Dimers, Zinc Dimer, and Zinc-Rare-Gas Dimers. *J. Phys. Chem. A* **2006**, *110*, 5121−5129.
(52) Zhao, Y.; Truhlar, D. G. Density Functional for Spectroscopy: No Long-Range Self-Interaction Error, Good Performance for Rydberg and Charge-Transfer States, and Better Performance on Average Than B3LYP for Ground States. *J. Phys. Chem. A* **2006**, *110*, 13126−13130.
(53) Peverati, R.; Truhlar, D. G. M11-L: A Local Density Functional That Provides Improved Accuracy for Electronic Structure Calculations in Chemistry and Physics. *J. Phys. Chem. Lett.* **2012**, *3*, 117−124.
(54) Peverati, R.; Truhlar, D. G. An Improved and Broadly Accurate Local Approximation to the Exchange−Correlation Density Functional: The MN12-L Functional for Electronic Structure Calculations in Chemistry and Physics. *Phys. Chem. Chem. Phys.* **2012**, *14*, 13171−13174.
(55) Haoyu, S. Y.; He, X.; Li, S. L.; Truhlar, D. G. MN15: A Kohn−Sham Global-Hybrid Exchange−Correlation Density Functional With Broad Accuracy for Multi-Reference and Single-Reference Systems and Noncovalent Interactions. *Chem. Sci.* **2016**, *7*, 5032−5051.
(56) Cohen, A. J.; Handy, N. C. Dynamic Correlation. *Mol. Phys.* **2001**, *99*, 607−615.
(57) Adamo, C.; Barone, V. Toward Reliable Density Functional Methods Without Adjustable Parameters: The PBE0 Model. *J. Chem. Phys.* **1999**, *110*, 6158−6170.
(58) Peverati, R.; Zhao, Y.; Truhlar, D. G. Generalized Gradient Approximation That Recovers the Second-Order Density-Gradient Expansion With Optimized Across-The-Board Performance. *J. Phys. Chem. Lett.* **2011**, *2*, 1991−1997.
(59) Peverati, R.; Truhlar, D. G. Communication: A Global Hybrid Generalized Gradient Approximation to the Exchange-Correlation Functional That Satisfies the Second-Order Density-Gradient Constraint and Has Broad Applicability in Chemistry. *J. Chem. Phys.* **2011**, *135*, No. 191102.
(60) Tao, J.; Perdew, J. P.; Staroverov, V. N.; Scuseria, G. E. Climbing the Density Functional Ladder: Nonempirical Meta−Generalized Gradient Approximation Designed for Molecules and Solids. *Phys. Rev. Lett.* **2003**, *91*, No. 146401.
(61) Staroverov, V. N.; Scuseria, G. E.; Tao, J.; Perdew, J. P. Comparative Assessment of a New Nonempirical Density Functional: Molecules and Hydrogen-Bonded Complexes. *J. Chem. Phys.* **2003**, *119*, 12129−12137.
(62) Chai, J.-D.; Head-Gordon, M. Systematic Optimization of Long-Range Corrected Hybrid Density Functionals. *J. Chem. Phys.* **2008**, *128*, No. 084106.
(63) Chai, J.-D.; Head-Gordon, M. Long-Range Corrected Hybrid Density Functionals With Damped Atom−Atom Dispersion Corrections. *Phys. Chem. Chem. Phys.* **2008**, *10*, 6615−6620.
(64) Grimme, S. Supramolecular Binding Thermodynamics by Dispersion-Corrected Density Functional Theory. *Chem. - Eur. J.* **2012**, *18*, 9955−9964.
(65) Li, Y.-P.; Gomes, J.; Mallikarjun Sharada, S.; Bell, A. T.; Head-Gordon, M. Improved Force-Field Parameters for QM/MM Simulations of the Energies of Adsorption for Molecules in Zeolites and a Free Rotor Correction to the Rigid Rotor Harmonic Oscillator Model for Adsorption Enthalpies. *J. Phys. Chem. C* **2015**, *119*, 1840−1850.
(66) Kozuch, S.; Shaik, S. How to Conceptualize Catalytic Cycles? The Energetic Span Model. *Acc. Chem. Res.* **2011**, *44*, 101−110.
(67) Although we note the large difference in magnitude between $\Delta E^{\ddagger}$ and $\Delta G^{\ddagger}$ due to a change in molecularity between the TDI and TDTS, the approximation $\Delta\Delta G^{\ddagger} \approx \Delta\Delta E^{\ddagger}$ remains valid as the translational Sackur-Tetrode entropy responsible for the large difference in magnitude cancels out when taking the difference.

https://doi.org/10.1021/acs.jpcc.3c03888
J. Phys. Chem. C 2023, 127, 16891−16900